

Self-sustained activity in balanced networks with low firing-rate

F. S. Borges^{1,2,*}, P. R. Protachevicz³, R. F. O. Pena⁴, E. L. Lameu^{5,6}, F. S. Matias^{7,8}, G. S. V. Higa¹, A. H. Kihara¹, C. G. Antonopoulos⁹, K. C. Iarosz^{2,6,10}, R. De Pasquale¹¹, A. C. Roque⁴, A. M. Batista^{3,10,12}, P. Ji¹³

¹ Center for Mathematics, Computation, and Cognition, Federal University of ABC, São Bernardo do Campo, SP, Brazil

² Institute of Physics, University of São Paulo, São Paulo, SP, Brazil

³ Graduate in Science Program - Physics, State University of Ponta Grossa, PR, Brazil

⁴ Laboratory of Neural Systems, Department of Physics, University of São Paulo, Ribeirão Preto, SP, Brazil

⁵ National Institute for Space Research, São José dos Campos, SP, Brazil

⁶ Department of Physics, Humboldt University, Berlin, Germany

⁷ Cognitive Neuroimaging Unit, CEA DRF/I2BM, INSERM, Université Paris-Sud, Université Paris-Saclay, F-91191 Gif/Yvette, France

⁸ Institute of Physics, Federal University of Alagoas, Maceió, AL, Brazil

⁹ Department of Mathematical Sciences, University of Essex, Wivenhoe Park, UK

¹⁰ Potsdam Institute for Climate Impact Research, Potsdam, Germany

¹¹ Department of Physiology and Biophysics, ICB, University of São Paulo, São Paulo, SP, Brazil

¹² Department of Mathematics and Statistics, State University of Ponta Grossa, Ponta Grossa, PR, Brazil

¹³ Institute of Science and Technology for Brain-Inspired Intelligence, Fudan University, Shanghai, China

arXiv:1809.01020v2 [q-bio.NC] 10 Sep 2018

Abstract

The brain can display self-sustained activity (SSA), which is persistent firing of neurons in the absence of external stimuli. This spontaneous activity shows low neuronal firing rates and is observed in diverse *in vitro* and *in vivo* situations. In this work, we study the influence of excitatory/inhibitory balance, connection density, and network size on the self-sustained activity of a neuronal network model. We build a random network of adaptive exponential integrate-and-fire (AdEx) neuron models connected through inhibitory and excitatory chemical synapses. The AdEx model mimics several behaviours of biological neurons, such as spike initiation, adaptation, and bursting patterns. In an excitation/inhibition balanced state, if the mean connection degree (K) is fixed, the firing rate does not depend on the network size (N), whereas for fixed N , the firing rate decreases when K increases. However, for large K , SSA states can appear only for large N . We show the existence of SSA states with similar behaviours to those observed in experimental recordings, such as very low and irregular neuronal firing rates, and spike-train power spectra with slow fluctuations, only for balanced networks of large size.

Keywords: self-sustained activity, neuronal networks, irregular firing activity

PACS: 87.10.Hk, 87.19.lj, 87.19.lm

1. Introduction

Self-sustained activity (SSA), where neurons display persistent activity even in the absence of external stimuli (Greicius, 2003; Fox, 2005), is observed in diverse situations such as *in vitro* cortical culture and slice preparations (Plenz, 1996; Sanchez-Vives, 2000; Shu, 2003), *in vivo* cortical slab preparations (Timofeev et al., 2000), slow-wave sleep (Steriade, 2001), anesthesia (Steriade, 1993), and resting state (Arieli, 1995; Mantini, 2007). Electrophysiological recordings of SSA states show irregular neuronal spiking, typically with low average frequencies of a few Hz but obeying long-tailed distributions (Hromádka, 2008;

O'Connor, 2010; Buzsáki & Mizuseki, 2014).

Many works have modeled neuronal networks with SSA by using random networks composed of excitatory and inhibitory leaky integrate-and-fire (LIF) neurons with external background input (Brunel, 2000; Vogels, 2005a; Parga, 2007; Kumar, 2008; Kriener, 2014; Ostojic, 2014). Other studies have considered networks with non-random architectures, composed of LIF neurons (Renart, 2007; Kaiser, 2010; Wang, 2011; Litwin, 2012; Potjans, 2014) or non-linear two-dimensional integrate-and-fire neuron models (Compte, 2006; Izhikevich, 2008; Destexhe, 2009; Stratton, 2010; Tomov, 2014, 2016). Both the architecture and the neuron types that comprise the network play an impor-

tant role in SSA states. SSA states are generated and maintained by recurrent interactions within networks of excitatory and inhibitory neurons. A stable SSA state is related to strong recurrent excitation within the neuronal network, which is restrained by inhibition to prevent runaway excitation. The balance between excitation and inhibition in neuronal networks is considered critical to maintain a SSA state (van Vreeswijk, 1996; Brunel, 2000; Shu, 2003; Haider, 2006; Taub, 2013).

In this work, we verify the existence of SSA in a random network composed of neurons with different intrinsic firing patterns (the so-called electrophysiological classes (Contreras, 2004)). We consider the adaptive exponential integrate-and-fire (AdEx) (Brette, 2005) model with cortical neurons modeled as regular spiking (RS) cells with spike frequency adaptation and fast-spiking (FS) cells with a negligible level of adaptation. In this type of network, depending on the excitatory synaptic strength, neurons can exhibit a transition from spiking to bursting synchronisation (Borges, 2017). Here, we show some conditions in that unstructured, sparsely connected networks of AdEx neurons can display low frequency self-sustained activity.

We show that not only the balance between excitation and inhibition but also the connection density and the network size are both important for low frequency self-sustained activity. In balanced networks, large values of mean node-degree connectivity are necessary to have low mean neuronal firing-rates, and for such values, large networks are necessary to have SSA states. In our simulations, we obtain similar results to the ones observed in experimental recordings, such as very low and irregular neuronal firing-rates (≈ 1 Hz) and spike-train power spectra with slow fluctuations (Litwin, 2012).

The paper is organised as follows: the introduction of the coupled AdEx network model were given in Section 2. In Section 3, we discuss the methodology for quantifying SSA in networks. Our results were presented in Section 4. Finally, the discussion and conclusion were given in Section 5.

2. Neuronal network model

We build a random neuronal network of N neurons by connecting them with probability p , where p is the probability that any two neurons in the network are connected, excluding autapses. The N neurons in the network are split into excitatory and inhibitory neurons according to the ratio 4 : 1, respectively. The connection probability p and the mean connection degree K of the network are associated by means of the relation

$$p = \frac{K}{(N-1)}. \quad (1)$$

The dynamics of each AdEx neuron $i = 1, \dots, N$ in the

network is given by (Destexhe, 2009)

$$\begin{aligned} C \frac{dV_i}{dt} &= -g_L(V_i - E_L) + g_L \Delta_T \exp\left(\frac{V_i - V_T}{\Delta_T}\right) \\ &\quad - \frac{1}{S} \left(w_i + \sum_{j=1}^N g_{ij}(V_i - E_j) + \Gamma_i \right), \quad (2) \\ \tau_w \frac{dw_i}{dt} &= a(V_i - E_L) - w_i \end{aligned}$$

where V_i and w_i are, respectively, the membrane potential and adaptation current of neuron i , g_{ij} is the synaptic conductance of the synapse from neuron j to neuron i , and Γ_i is the external perturbation applied to neuron i . The meanings of the other parameters in Eq. (2) are defined in Table 1. The synaptic conductance g_{ij} has exponential decay with synaptic time-constant τ_s . The values of the parameters were selected in order to reproduce the spiking characteristics of RS (excitatory) and FS (inhibitory) neurons (Destexhe, 2009). They are shown in Table 1.

When the membrane potential of neuron i is above a threshold potential ($V_i(t) > V_{\text{thres}} = 20$ mV), the neuron is assumed to generate a spike and the following update conditions are applied

$$\begin{aligned} V_i &\rightarrow V_r = -60 \text{ mV}, \\ w_i &\rightarrow w_i + b, \\ g_{ji} &\rightarrow g_{ji} + g_s, \end{aligned} \quad (3)$$

where V_r is the reset potential. The update parameters b and g_s have different values for excitatory ($b = 0.01$ nA and g_{ex}) and inhibitory ($b = 0$ and g_{in}) neurons. The g_{ji} updates have synaptic delays 1.5 ms and 0.8 ms for excitatory and inhibitory synapses, respectively. After the update, g_{ji} decays exponentially with a fixed time constant τ_s (5 ms for excitatory and 10 ms for inhibitory synapses (Wang, 2011)). We define the relative inhibitory conductance $g = g_{\text{in}}/g_{\text{ex}}$ to be used as a parameter in the investigation of network dynamics. In each simulation, we apply external stimuli Γ to 5% of the N neurons (randomly chosen) for 50 ms to initiate network activity, and then we stop the external stimuli to observe the activity, which can be persistent (SSA) or transient. For each neuron i , the external stimulus Γ_i has the same characteristics: it consists of excitatory current pulses with synaptic conductances that rise instantaneously to $0.01 \mu\text{S}$ and decay exponentially afterwards with decay time 5 ms, generated by a homogeneous Poisson process with rate 400 Hz.

3. Methodology

3.1. Coefficient of variation

In this work, we use different statistical measures based either on time intervals or spike times. Those based on time intervals exploit the inter-spike interval (ISI) where the m th interval is defined as the difference between two

Table 1: Values of parameters used in the neuron model in Eq. (2). Values for excitatory neurons are indicated by \bullet , and for inhibitory by \ast . The ranges are indicated by square brackets.

Parameter	Symbol	Value
Membrane capacitance	C	$1 \mu\text{F}/\text{cm}^2$
Resting leak conductance	g_L	$0.05 \text{mS}/\text{cm}^2$
Resting potential	E_L	-60mV
Slope factor	Δ_T	2.5mV
Spike threshold	V_T	-50mV
Membrane area	S	$20,000 \mu\text{m}^2$
Refractory time period	t_r	2.5ms
Adaptation intensity	a	$0.001 \mu\text{S}$
Adaptation time constant	τ_w	600ms
Integration time step	h	10^{-2}ms
Time	t	$[0,10] \text{s}$
Reversal potential	E_j	$0 \text{mV} \bullet$ $-80 \text{mV} \ast$
Synaptic time constant	τ_s	$5 \text{ms} \bullet$ $10 \text{ms} \ast$
Synaptic conductance	g_s	$[0,12] \text{nS} \bullet$ $[0,240] \text{nS} \ast$
Synaptic delay	d	$1.5 \text{ms} \bullet$ $0.8 \text{ms} \ast$

consecutive spike times t_i^m and t_i^{m+1} of neuron i , namely $\text{ISI}_i = t_i^{m+1} - t_i^m > 0$. The ratio between the standard deviation and the mean (indicated by $\langle \cdot \rangle$) is defined as the coefficient of variation of the ISIs

$$\text{CV}_i = \frac{\sqrt{\langle (\text{ISI}_i - \langle \text{ISI}_i \rangle)^2 \rangle}}{\langle \text{ISI}_i \rangle}, \quad (4)$$

for the i th neuron.

3.2. Firing-rate

We define the spike-train of neuron i as the sum of delta functions (Gabbiani, 1998)

$$x_i(t) = \sum_{[t_i^m]} \delta(t - t_i^m), \quad (5)$$

where $[t_i^m]$ is the set of all spike times of neuron i for $t \in [0, T]$. Based on Eq. (5), we calculate the mean firing rate of neuron i over the time interval $[0, T]$ as

$$\bar{F}_i = \frac{1}{T} \int_0^T x_i(t) dt. \quad (6)$$

For all neurons in the network, we define the time-varying network firing rate (in Hz) in intervals of 1 ms as

$$F(t) = \frac{1000}{N} \sum_{i=1}^N \left(\int_t^{t+1\text{ms}} \delta(t - t_i^m) dt \right), \quad (7)$$

and the mean network firing rate over the time interval $[0, T]$ as

$$\bar{F} = \frac{1000}{N} \sum_{i=1}^N \left(\frac{1}{T} \int_0^T \delta(t - t_i^m) dt \right) = \frac{1}{\langle \text{ISI} \rangle}, \quad (8)$$

where $\langle \text{ISI} \rangle$ is the mean ISI of the network given by

$$\langle \text{ISI} \rangle = \frac{1}{N} \sum_{i=1}^N \langle \text{ISI}_i \rangle. \quad (9)$$

3.3. Power spectrum

From the definition of spike-train in Eq. (5), we define the power spectrum of neuron i by

$$S_i^{xx}(f) = \frac{\langle \tilde{x}_i(f) \tilde{x}_i^*(f) \rangle}{T}, \quad (10)$$

where $\langle \cdot \rangle$ indicates ensemble average, $[0, T]$ is the time window of the simulation, $\tilde{x}_i(f)$ is the Fourier transform of neuron i , given by $\tilde{x}_i(f) = \int_0^T e^{2\pi i f t} x_i(t) dt$, and $\tilde{x}_i^*(f)$ is the complex conjugate of $\tilde{x}_i(f)$. The power spectrum of a set of M ($M \leq N$) neurons, $\bar{S}^{xx}(f)$ is then defined as the average power spectrum of these M neurons

$$\bar{S}^{xx}(f) = \frac{1}{M} \sum_{i=1}^M S_i^{xx}(f). \quad (11)$$

In order to keep consistency over the different simulations (see Fig. 5), we choose $M = 5 \times 10^4$ independently of the values of N and K . Here, we will use two measures related to \bar{S}^{xx} to describe spike-train characteristics (Lindner, 2009; Grün, 2010; Wieland, 2015; Pena, 2018).

The first one is the Fano factor $FF = \langle \Delta n^2 \rangle / \langle n \rangle$, which is defined as the ratio of the variance to the mean of the spike count of the M neurons over the time window $[0, T]$, $n = \sum_{i=1}^M \int_0^T dt x_i(t)$. Its relation to \bar{S}^{xx} is meaningful in the vanishing frequency limit of $\bar{S}^{xx}(f)$, i.e. $\lim_{f \rightarrow 0} \bar{S}^{xx}(f) = \bar{F} \cdot FF$. The Fano factor FF is a standard measure of neuronal variability ($FF = 1$ for a Poisson process) and is related to the CV of the ISIs of the M neurons (Cox, 1966) by $\lim_{f \rightarrow 0} \bar{S}^{xx}(f) = \bar{F} \cdot \text{CV}^2 (1 + 2 \sum_{k=1}^{\infty} r_k)$, where r_k is the serial correlation coefficient between ISIs that are lagged by k .

The second one is the mean firing-rate of the M neurons, \bar{F}_M (defined as in Eq. (8) but dividing by M), which is related to $\bar{S}^{xx}(f)$ by its limit to infinity, i.e. $\lim_{f \rightarrow \infty} \bar{S}^{xx}(f) = \bar{F}_M$.

3.4. Synaptic input

The instantaneous synaptic conductance of neuron i due to all excitatory and inhibitory synapses arriving to it will be written here as

$$G_i(t) = \sum_{j \in \mathfrak{E}} g_{ij}(t) + \sum_{j \in \mathfrak{I}} g_{ij}(t) = G_{ex,i}(t) + G_{in,i}(t), \quad (12)$$

where \mathfrak{E} and \mathfrak{I} are the sets of all excitatory and inhibitory neurons in the network, respectively.

The instantaneous synaptic input to neuron i will be written as

$$I_{\text{syn},i}(t) = \sum_{j \in \mathcal{E}} g_{ij}(E_j - V_i) + \sum_{j \in \mathcal{I}} g_{ij}(E_j - V_i) \quad (13)$$

$$= I_{\text{syn},i}^E(t) + I_{\text{syn},i}^I(t),$$

and the mean synaptic input I_{syn} to all neurons in the network over simulation time $[0, T]$ as

$$\bar{I}_{\text{syn}} = \frac{1}{N} \sum_{i=1}^N \frac{1}{T} \int_{t=0}^T (I_{\text{syn},i}^E(t) + I_{\text{syn},i}^I(t)) dt. \quad (14)$$

3.5. Network decay-time

Finally, for a given neuron i we define the time of its last spike as the maximum time in its spike train

$$t_i^{\text{last}} = \max \{t_i^m\}. \quad (15)$$

The network decay-time (DT) is defined as the last spike in the network during simulation time, i.e. the maximum t_i^{last} comparing all neurons in the network,

$$\text{DT} = \max \{t_i^{\text{last}}, i = 1, \dots, N\}. \quad (16)$$

3.6. Implementation details

All simulations were implemented in C. The ordinary differential equations were integrated by the fourth order Runge-Kutta method with step size 0.01 ms.

3.7. Experimental details

3.7.1. Animals

Electrophysiological experiments were conducted using male Wistar rats with 20-25 postnatal days. All animal were kept cycle in an animal facility in a 12:12h light/dark cycle with temperature adjusted for $23^\circ\text{C} \pm 2^\circ$ with free access to food and water. All procedures were approved by the Institutional Animal Care Committee of the Institute of Biomedical Sciences, University of São Paulo (CEUA ICB/USP n. 090, fls. 1°).

3.7.2. Brain slices preparation

After animals were deeply anesthetised through isoflurane inhalation (AErrane; Baxter Pharmaceuticals) they were decapitated and the brain was quickly removed and submerged in cooled (0°C) oxygenated (5% CO_2 - 95% O_2) cutting solution (in mM): 206 sucrose, 25 NaHCO_3 , 2.5 KCl, 10 MgSO_4 , 1.25 NaH_2PO_4 , 0.5 CaCl_2 , and 11 D-glucose. After removing the cerebellum, brain hemispheres were separated by a single sagittal cut. Both brain hemispheres were trimmed up and glued in a metal platform and sectioned using a vibratome (Leica - VT1200). 350-400 μm brain slices were obtained by advancing the vibratome blade from anterior-posterior orientation. Slices were rapidly transferred to a holding chamber containing artificial cerebrospinal fluid (ACSF; in mM): 125 NaCl, 25

NaHCO_3 , 3 KCl, 1.25 NaH_2PO_4 , 1 MgCl_2 , 2 CaCl_2 , and 25 D-glucose. Slices were kept oxygenated at room temperature (20 - 25°) for at least one hour before proceeding with electrophysiological recordings.

3.7.3. Electrophysiological recordings

Brain slices containing the hippocampal formation were placed in a submersion-type recording chamber upon a modified microscope stage and maintained at 30°C with constant perfusion of oxygenated ACSF (5% CO_2 -95% O_2). Whole-cell recordings were made from neurons located in the pyramidal layer of CA1. Recording pipettes were fabricated from borosilicate glass (Garner Glass) with input resistances of ~ 4 -6 $\text{M}\Omega$ and were filled with intracellular solution (in mM): 135 K-gluconate, 7 NaCl, 10 HEPES, 2 Na_2ATP , 0.3 Na_3GTP , 2 MgCl_2 ; at a pH of 7.3 obtained with KOH and osmolality of 290 mOsm. All experiments were performed using a visualised slice setup under a differential interference contrast-equipped Nikon Eclipse E600FN microscope. Recordings were made by using a Multiclamp 700B amplifier and pClamp software (Axon Instruments). Only recordings from cells that presented spontaneous activity with membrane potentials lower than -60 mV, access resistance lower than 20 $\text{M}\Omega$, and input resistance higher than 100 $\text{M}\Omega$ and lower than 1000 $\text{M}\Omega$ were included in our data. We injected depolarising currents to identify regular, tonic, or bursting spike patterns. Neuronal spontaneous activity was assessed by 10 minutes of continuous recordings in current clamp mode.

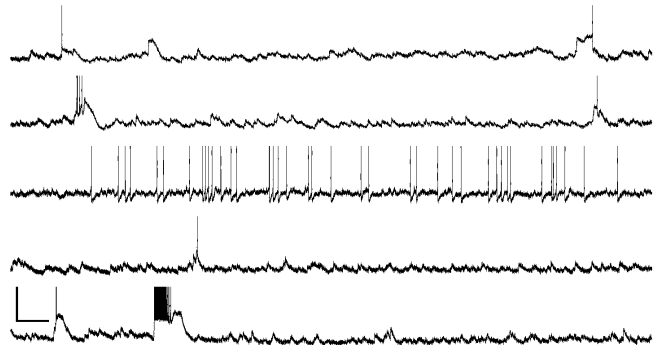


Figure 1: Intracellular recordings demonstrating a high variability of spontaneous activity pattern. Twenty seconds of recordings are shown (horizontal black bar denotes 1 s and vertical black bar denotes 50 mV).

4. Self-sustained activity

SSA assessed by electrophysiological recordings in physiological brain states is characterised by irregular neuronal spiking, normally with low average frequency fitted in long-tailed distribution (Buzsáki & Mizuseki, 2014). Interestingly, some brain regions are able to produce spontaneous network activity after slicing procedure including hippocampal sharp waves (Maier, 2003; Giannopoulos, 2013; Bazelot, 2016). Once hippocampus slices present

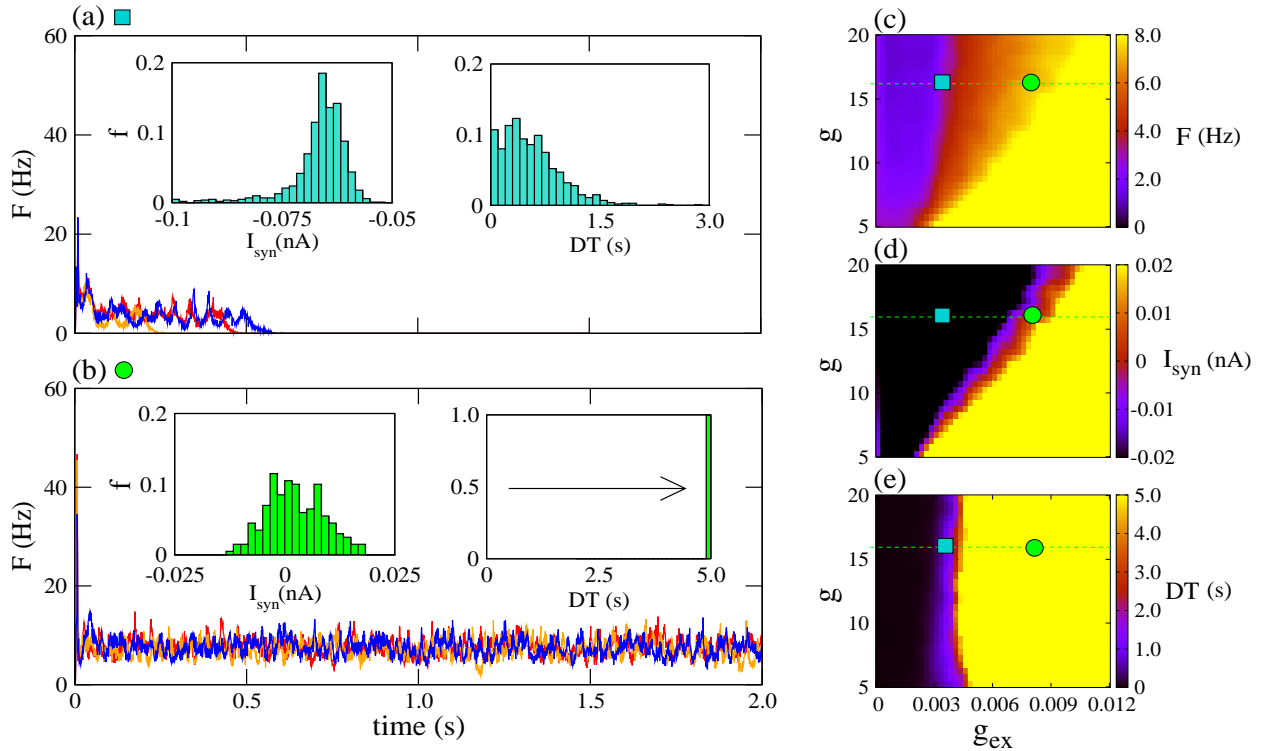


Figure 2: (Colour online) Self-sustained activity (SSA) emerges due to the excitatory/inhibitory balance in the network. Time-dependent network firing rate (F) in two different regimes: (a) non-SSA and (b) SSA. Each trace corresponds to a different simulation. The two neuronal networks have the same set of parameters except that the excitatory conductance is (a) $g_{\text{ex}} = 0.0035 \mu\text{S}$ and (b) $g_{\text{ex}} = 0.008 \mu\text{S}$. The insets show the probability distribution, over 10^3 simulations, of the mean synaptic inputs (\bar{I}_{syn}) and decay-times (DT) in each case. (c) Mean network firing rate (\bar{F}), (d) mean synaptic input (\bar{I}_{syn}), and (e) decay-time (DT) as a function of excitatory (g_{ex}) and relative inhibitory synaptic coupling (g). The neuronal network has $N = 10^4$ neurons and connection probability $p = 0.02$. In (a) and (b), we fixed $g = 16$. The turquoise squares correspond to the parameters in (a) and the green circles to those in (b).

SSA represented by spontaneous activity, we used CA1 neurons whole cell recording to demonstrate the possible variability of firing rate pattern observed in the brain. Our intracellular recordings demonstrated a high variability of spontaneous activity pattern including low neuronal firing-rates and small bursts activity in distinct recorded neurons. In Fig. 1, we show a representation of five traces obtained by whole-cell patch clamp from CA1 neurons for 20 seconds. Recorded neurons presented distinct firing pattern including very low firing (0.018 Hz) to small bursts of spikes (see the second and last trace in Fig. 1). In the whole record (600 s), the mean firing rate over the five neurons is ≈ 1.172 Hz (0.028, 0.157, 3.403, 0.018, 2.252). Similar firing patterns, with high variability and low neuronal firing-rates, are found in different recordings in the hippocampus and cortex in the rat brain during slow-wave sleep (Mizuseki, 2013), and recordings of human middle temporal gyrus during sleep (Peyrache, 2012).

In order to reproduce SSA firing patterns with low neuronal firing-rates, we analyse the parameter space $g_{\text{ex}} \times g$ for a neuronal network of $N = 10^4$ neurons and connection probability $p = 0.02$. We focus on an area of parameter space where we found a balanced regime between excitation and inhibition. In this area we do not observe SSA

for $g_{\text{ex}} < 0.004 \mu\text{S}$, which is the weak coupling region. Examples of time-dependent network firing rates in this region are shown in Fig. 2(a), for $g_{\text{ex}} = 0.0035 \mu\text{S}$ and $g = 16$. The initial stimulus applied in the first 50 ms generates short-lived activity in the network. The mean synaptic input to the network neurons \bar{I}_{syn} is essentially negative (left-hand inset in Fig. 2(a)) and the network decay-time DT is always less than 3 s (right-hand inset in Fig. 2(a)). Examples of time-dependent network firing rates in the region of SSA are shown in Figure 2(b), corresponding to parameters $g_{\text{ex}} = 0.008 \mu\text{S}$ and $g = 16$. The mean synaptic input is approximately balanced ($\bar{I}_{\text{syn}} \approx 0$) and the decay-time is higher than the maximum time used in our simulations ($\text{DT} \geq 5$ s).

For $N = 10^4$ neurons, the lowest mean network firing rates are approximately 2 Hz. The region where these rates occur is shown in purple in Fig. 2(c). A particular case for $g_{\text{ex}} < 0.003 \mu\text{S}$ is indicated by a turquoise square, where the activity is not self-sustained. For the random network and parameter space considered, the region with SSA is roughly determined by $g_{\text{ex}} > 0.004 \mu\text{S}$ (indicated in yellow in Fig. 2(e)). The lowest mean network firing rate of an SSA state is around 4 Hz (red region in Fig. 2(c)). Within this region, one can identify the

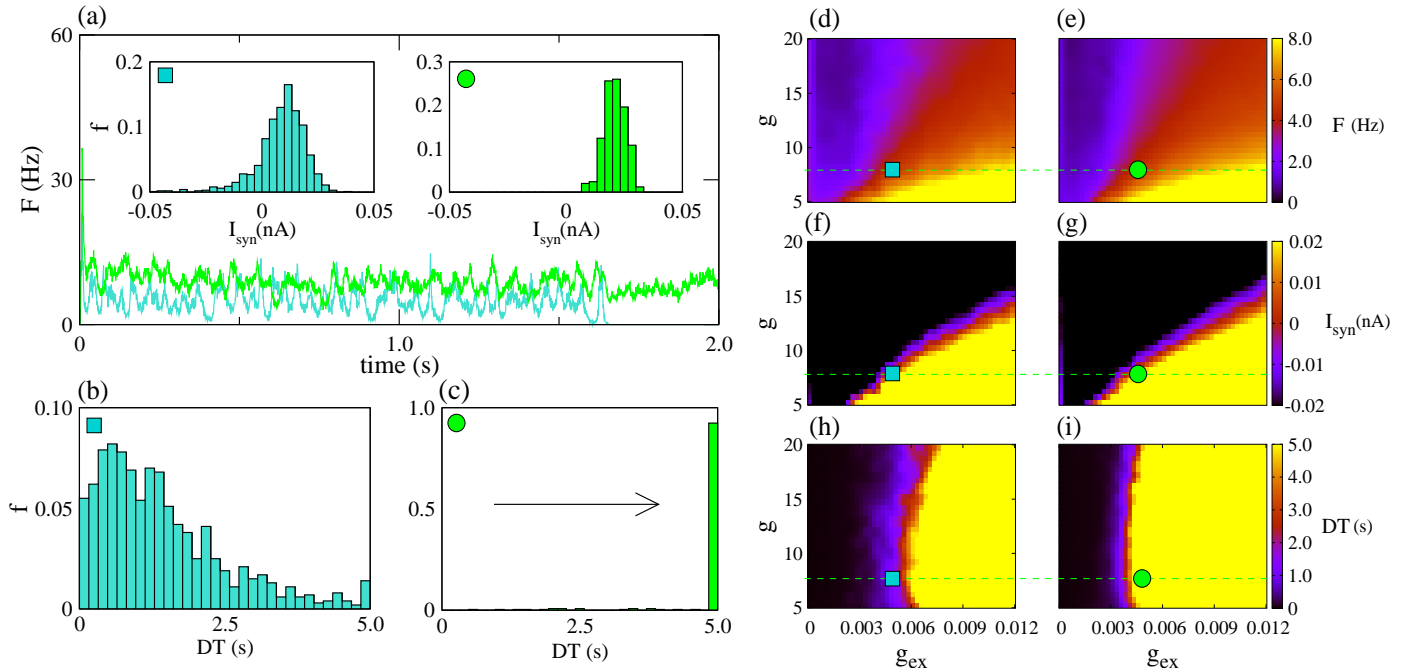


Figure 3: (Colour online) Effect of network size in SSA. (a) Time-dependent network firing rate (F) for $N = 10^4$ (turquoise line) and $N = 2 \times 10^4$ (green line). The insets show the probability distribution, over 10^3 simulations, of the mean synaptic input (\bar{I}_{syn}) for each case. (b) and (c) decay-time (DT) distribution (also for 10^3 simulations) for $N = 10^4$ and $N = 2 \times 10^4$ (colours follow the same convention as in (a)). We considered the excitatory conductance $g_{\text{ex}} = 0.005 \mu\text{S}$, mean degree of connection $K = 400$, and relative inhibitory synaptic coupling $g = 8$. The mean network firing rate (d) and (e), mean synaptic input (f) and (g), and mean decay-time (h) and (i) are shown as a function of g_{ex} and g for $N = 10^4$ (left) and $N = 2 \times 10^4$ (right), respectively. The turquoise squares correspond to $N = 10^4$ and $p = 0.04$, and the green circles to $N = 2 \times 10^4$ and $p = 0.02$.

region of excitation/inhibition balance by considering the region with $I_{\text{syn}} \approx 0$ (see Eq. (14)). This is shown in red in Fig. 2(d). The black and yellow regions in Fig. 2(d) correspond to slightly predominant inhibitory and excitatory mean synaptic input, respectively. A SSA case with $\bar{F} \approx 4$ Hz and excitation/inhibition balance is indicated by the green circle in Figs. 2(c)-(e) and corresponds to $g_{\text{ex}} = 0.008 \mu\text{S}$ and $g = 16$.

To study the effect of the size of the network on SSA, we considered two networks of different sizes but same mean degree. The first has $N = 10^4$ and $p = 0.04$ and the second $N = 2 \times 10^4$ and $p = 0.02$, with both having $K = 400$. The parameters ($g_{\text{ex}} = 0.005 \mu\text{S}$ and $g = 8$) are the same for the two networks, and put them close to the balanced state. In Fig. 3(a), we show the time evolution of the firing rates of the two networks. For $N = 10^4$ (turquoise line), the activity decays before 2 s, and for $N = 2 \times 10^4$ (green line) SSA is observed. The distributions of \bar{I}_{syn} for the two cases (see the insets in Fig. 3(a)) have similar (positive) average values but the one for $N = 10^4$ is broader and left-skewed. The decay-time distribution (Figs. 3(b), (c)) clearly shows that the networks with $N = 2 \times 10^4$ have SSA, while the ones with $N = 10^4$ are predominantly short-lived. A comparison of networks with the two sizes in the $g_{\text{ex}} \times g$ parameter space is shown in Figs. 3(d)-(i). The mean network firing rate and mean synaptic input display similar behaviour in the parameter space for the two net-

work sizes (Figs. 3(d)-(g)). However, this similarity is not seen in the diagram for DT (Figs. 3(h)-(i)). The region corresponding to SSA (yellow in the diagrams) is larger for $N = 2 \times 10^4$ than for $N = 10^4$. Moreover, the shape of this region for $N = 2 \times 10^4$ discloses almost absent sensitivity of SSA duration to the relative inhibitory synaptic conductance g . On the other hand, for $N = 10^4$ the SSA lifetime is sensitive to g for $0.006 \mu\text{S} \lesssim g_{\text{ex}} \lesssim 0.008 \mu\text{S}$, and only for strong coupling ($g_{\text{ex}} \gtrsim 0.008 \mu\text{S}$), it becomes insensitive to g .

Next, we investigate the influence of the network parameters N , p , and K (Eq. (1)) on the network firing rate of SSA states. In order to do so, we fix $g_{\text{ex}} = 0.008 \mu\text{S}$ and $g = 16$ to keep the network around excitatory/inhibitory balance. Figure 4 shows the mean network firing rate of SSA states (colour scale) in the parameter space $N \times p$. Moreover, the white area in the diagram corresponds to non-SSA states. We can see that the mean network firing rate of SSA states depends on both N and p . In particular, low firing rate SSA states appear when the network size N increases. The black solid line in Fig. 4 represents networks with mean node-degree $K = 1500$, in which case there are SSA states for $N \geq 1.5 \times 10^5$ neurons. The inset in Fig. 4(a) shows the dependence of the mean network firing rate \bar{F} of SSA states on the mean connection node-degree K for constant N . We can observe that lower rates are obtained as K increases. However, very low rates (\approx

1 Hz) are present only for very large network sizes. In the inset in Fig. 4(b), we can observe that the network size does not alter the mean network firing rate when K is kept constant. Therefore, large K plays an important role in the occurrence of low network firing rates, and for such low rates, large networks are necessary to support SSA states.

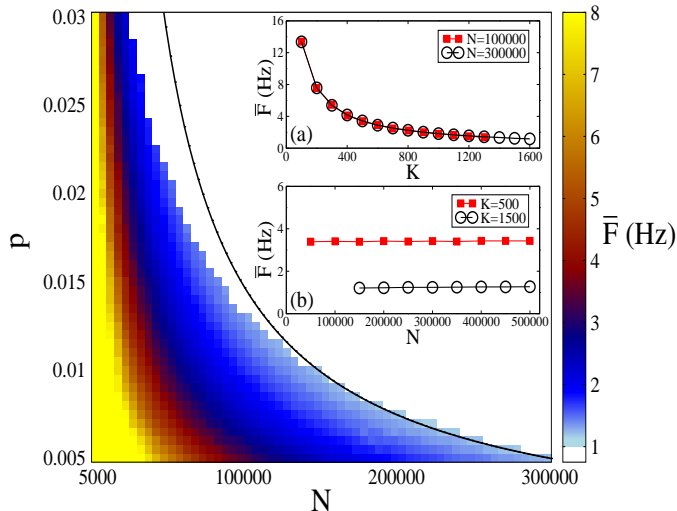


Figure 4: (Colour online) Mean SSA network firing rate \bar{F} (colour scale) as a function of the number of neurons N and connection probability p . Each point in the coloured part of the diagram gives \bar{F} calculated for a simulation of the network with the corresponding parameters. The white area in the diagram corresponds to non-SSA states. The black line represents networks with mean node-degree $K = 1500$ (according to Eq. (1)). Upper inset: mean network firing rate \bar{F} as a function of K keeping constant the number of neurons N , where the red squares and black circles represent $N = 1.0 \times 10^5$ and $N = 3.0 \times 10^5$ neurons, respectively. Lower inset: mean network firing rate \bar{F} as a function of N , showing independence of \bar{F} in relation to network size N for constant connection degree K , the curves represent two selected K values: $K = 500$ (red squares) and $K = 1500$ (black circles). We have used $g_{ex} = 0.008 \mu\text{S}$ and $g = 16$ for all simulations in this figure.

Figure 5 displays statistical results for three different combinations of network size and node-degree, namely ($N = 10^5$; $K = 1300$), ($N = 3 \times 10^5$; $K = 1500$), and ($N = 5 \times 10^5$; $K = 1700$). The time-varying network firing rate is non-periodic and its mean value decreases as both N and K increase (Fig. 5(a)). In the three cases, the spiking variability, characterised by the ISI distribution, is very well described by a Poisson distribution (Figs. 5 (c)-(e)). This is characteristic of irregular neuronal firing (Maimon, 2009; Gewaltig, 2013; Mochizuki, 2016). Moreover, the CV of the ISIs slowly converges to the one of a Poisson process ($= 1$) as both N and K increase.

As seen in Section 3.3, the spike-train power spectrum of a set of M neurons from the network is related to different statistics that characterise network firing. In our simulations, we can observe these relations by taking the limits of the power spectrum as $f \rightarrow \infty$ or $f \rightarrow 0$. In the $f \rightarrow \infty$ limit, $\bar{S}^{xx}(f)$ converges to the mean firing

rate of the M neurons, \bar{F}_M (a proxy to \bar{F}). In Fig. 5(b), one can see that these mean firing rates are very low ($1 \text{ Hz} \lesssim \bar{F}_M \lesssim 1.5 \text{ Hz}$), and the smaller rates occur for the larger N and K . On the other hand, irregularity is associated with vanishing frequency, namely $\lim_{f \rightarrow 0} \bar{S}^{xx}(f) = \bar{F}.FF$.

Assuming approximately the same \bar{F} for the three networks in Fig. 5(b), say $\bar{F} \approx 1.3$, the $f \rightarrow 0$ limit of $\bar{S}^{xx}(f)$ shows that $FF > 1$ for all of them. This suggests a process more irregular than the Poisson process (van Vreeswijk, 2004), e.g. bursting (Mochizuki, 2016). Moreover, as the network size N increases, FF decreases, indicating tendency to converge to a Poisson process and is linked to a standard irregularity measure and CV. We see that in the limit of very small frequencies, the value of the power spectra decreases as both K and N increases, confirming the behaviour observed by the CV, i.e. the spiking times are becoming more regular. The power spectra display slow fluctuations, which can be explained by the low neuronal firing rates and bursting spiking patterns (as discussed below). Slow power spectrum fluctuations are also a feature of spontaneous activity in cortical networks (Mantini, 2007; Wieland, 2015; Mastrogiuseppe, 2017).

In Fig. 6, we show characteristics of the SSA firing patterns with low rate exhibited by the network (a particular case with $N = 5 \times 10^5$ and $K = 1700$ is shown as a representative example). The patterns have sparse and non-synchronous activity (Fig. 6(a)), akin to what has been termed the heterogeneous variant (Ostojic, 2014) of the asynchronous irregular (AI) regime (Brunel, 2000; Vogels, 2005b). In the homogeneous AI regime, all neurons fire with the same mean rate, but in the heterogeneous AI regime, the mean firing rates fluctuate in time and across neurons. In some cases, neurons can even exhibit bursting periods (as can be seen in Fig. 6(b)). Neurons have low firing rates, with a right-skewed distribution that peaks around 1 Hz (Fig. 6(d)). Irregularity is confirmed by the CV of ISIs and power spectra analysis (Fig. 5). The similarity between the firing regime observed in our simulations and the heterogeneous AI state can be further verified by a comparison of the respective spike-train power spectra. Spectra for networks in heterogeneous AI states have been calculated elsewhere (Pena, 2018) and display slow fluctuations as shown here (Fig. 5(b)).

The distributions over neurons of the excitatory (G_{ex}) and inhibitory (G_{in}) synaptic conductances (panels (e) and (f) in Fig. 6) have nearly symmetric shapes, with the G_{in} distribution slightly right skewed, according to experimental evidence (Rudolph, 2007), though the conductance values are higher than in the experimental recordings. The distributions of excitatory (I_{syn}^E) and inhibitory (I_{syn}^I) synaptic inputs are nearly identical and vary over nearly the same range of absolute values, though the upper end of the range is slightly higher for the inhibitory synaptic inputs (panels (g) and (h) in Fig. 6). This is a hallmark of a balanced state, and the neuronal spikes happen due to the large synaptic conductance variability. This

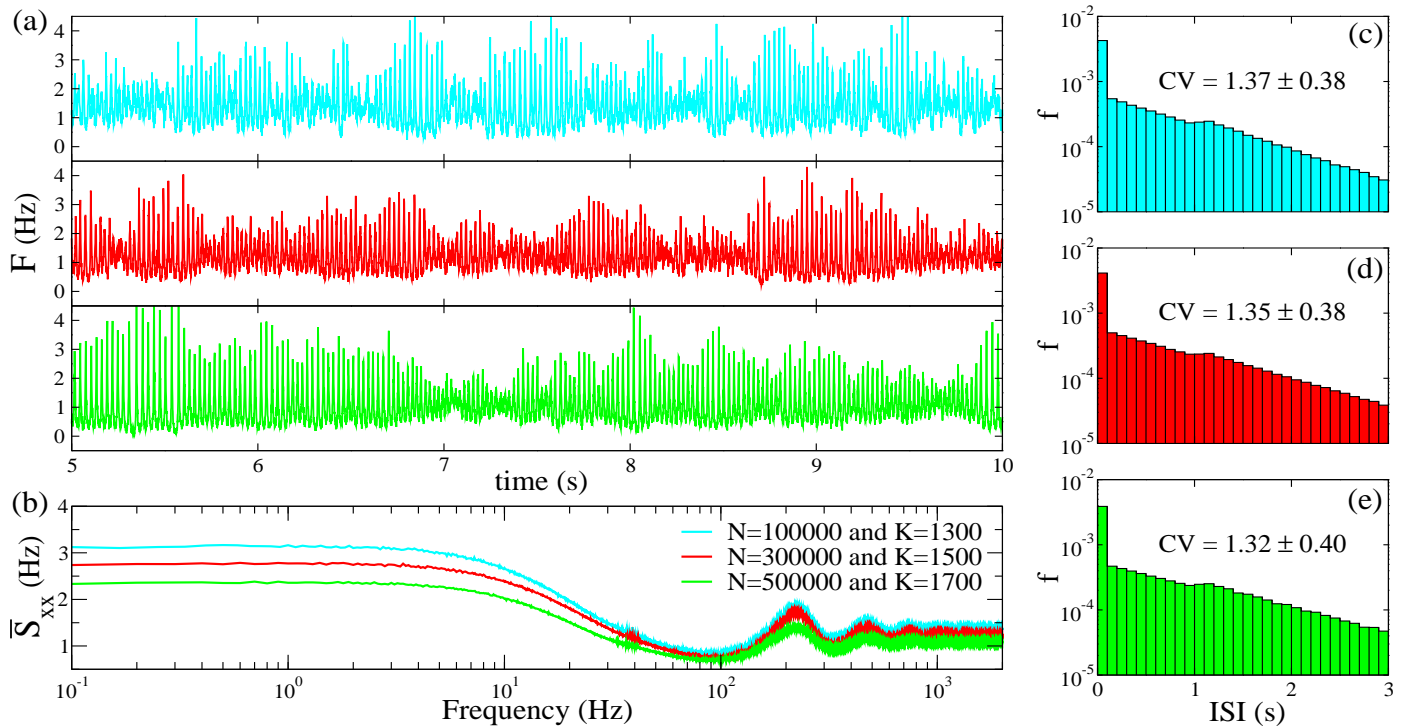


Figure 5: (Colour online) Statistical results for SSA as a function of N and node-degree K . (a) From top to bottom, we show F as N and K increase (for the N and K values, see legend in (b)). (b) Power spectra averaged over 5×10^4 neurons in the network and 10 s of simulation. Note that the horizontal axis is logarithmic and the vertical linear. (c)-(e) ISI distributions for the same three networks with the vertical axes in logarithmic and horizontal in linear scales. The corresponding CVs are indicated in the graphs. In the three cases, the parameter values are $g_{ex} = 0.008 \mu\text{S}$ and $g = 16$.

allows necessary conditions for the appearance of SSA.

5. Conclusion

In this paper, motivated by the self-sustained activity that is observed in the brain in the absence of external stimuli, we sought to study necessary conditions by which irregular and low-frequency self-sustained dynamics emerge in neuronal networks with random connectivity. We build neuronal networks of excitatory (80%) and inhibitory (20%) neurons where the neurons are randomly connected through chemical synapses and are mathematically described by the adaptive exponential integrate-and-fire model. This model mimics the behaviour of biological neurons, exhibiting spiking and bursting patterns of activity. We studied the network features by varying (i) the balance between excitation and inhibition, and (ii) the topological characteristics of the network. Results were obtained by running a large number of simulations in order to obtain valid statistical results and their firing rates.

Our results allowed us to observe neural activity with slow fluctuations in the absence of external perturbation. We found that the pattern of low firing-rate self-sustained activity is asynchronous and irregular as depicted in raster plots. We showed that the irregular spikes with low rate depend on the mean node degrees of the neurons, and that low-rate self-sustained activity occurs for a tight balance

between inhibition and excitation and large network sizes. When the connection mean degree (K) is fixed, the mean network firing rate does not change with the network size (N). In an excitation/inhibition balanced network, if N is fixed, the mean network firing rate decreases when K increases. However, there is a maximum K value for which it is possible to maintain SSA states, and this value is proportional to the network size. Therefore, large networks are necessary to have SSA states when K is large. Moreover, the spikes are due to the synaptic-conductance variability, and the inhibitory synaptic input is slightly higher than the excitatory. Our simulation results resemble those obtained from experimental recordings, such as irregular firing with network firing rate approximately equal to 1 Hz.

Finally, we have been able to verify the existence of low neuronal firing-rate SSA in the balanced network. This phenomenon is characterised by irregular network oscillations and shows that low frequency self-sustained activity can be found in large balanced random networks.

Acknowledgements

We wish to acknowledge the support from the following grants and schemes: CNPq (grants: 154705/2016-0, 306251/2014-0, 311467/2014-8, Universal 432429/2016-6), CAPES (grant 88881.120309/2016-01), FAPEAL, Interna-

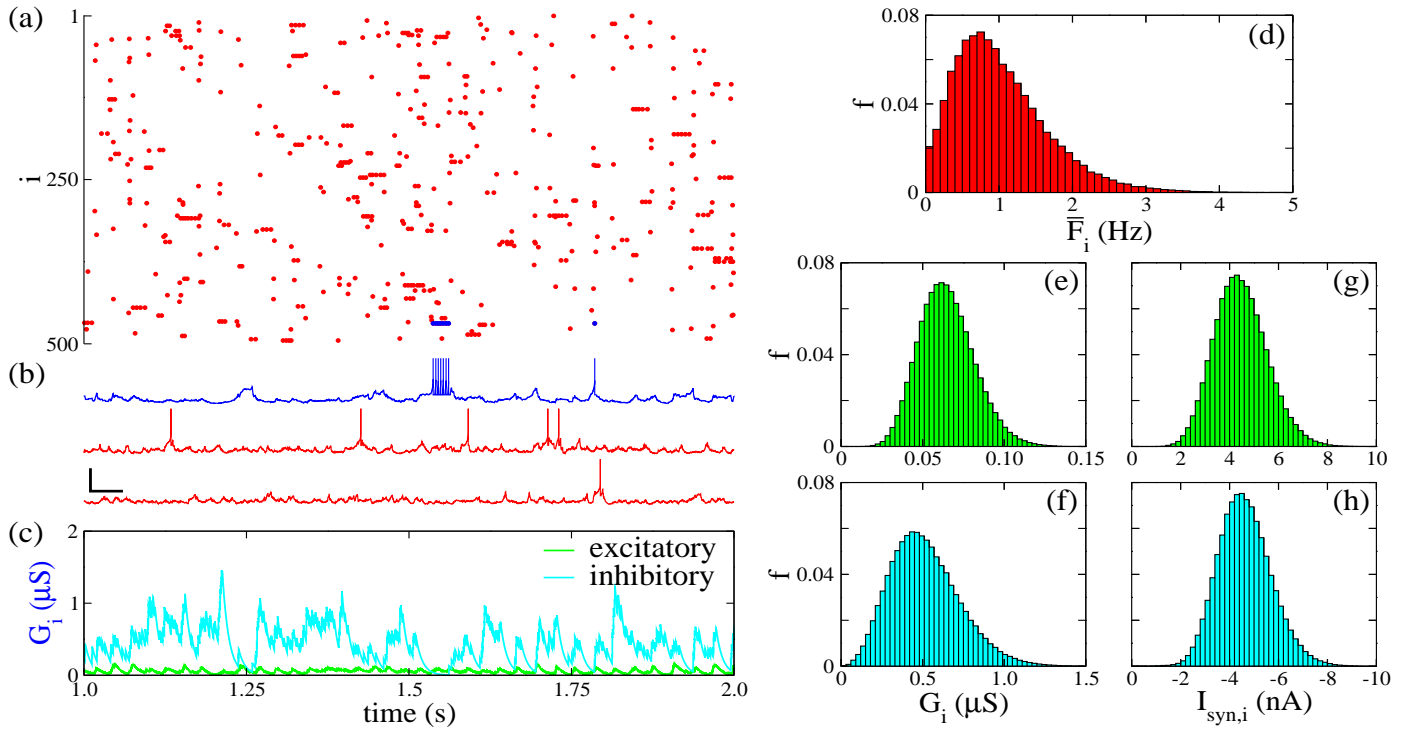


Figure 6: (Colour online) Characteristics of low firing-rate SSA states. All plots refer to a single simulation of a network with $N = 5 \times 10^5$, $K = 1700$, and parameters $g_{ex} = 0.008 \mu\text{S}$ and $g = 16$. (a) Raster plot of 2 s of simulation time (only 500 randomly chosen neurons from the network are shown). (b) membrane potential of three randomly chosen neurons from the network (horizontal black bar denotes 0.2 s and vertical black bar denotes 50 mV). (c) Time-varying synaptic conductances ($G_{ex,i}(t)$ in green and $G_{in,i}(t)$ in cyan) of neurons represented by blue line in (b). (d) distribution of mean firing rates \bar{F}_i (Eq. (6)) of all neurons in the network. Distribution of excitatory ($G_{ex,i}$) (e) and inhibitory ($G_{in,i}$) (f) synaptic conductances of all network neurons at the end of the simulation. Distribution of excitatory ($I_{syn,i}^E$) (g) and inhibitory ($I_{syn,i}^I$) (h) synaptic inputs of all network neurons at the end of the simulation.

tional Visiting Fellowships Scheme of the University of Essex, and FAPESP-São Paulo Research Foundation (grants: 2011/19296-1, 2013/07699-0 (NeuroMat), 2013/25667-8, 2015/50122-0, 2015/07311-7, 2016/23398-8, 2017/13502-5, 2017/18977-1, 2017/20920-8, 2017/26439-0, and TRP 2015/50122-0).

References

- Amit, D. J., & Brunel, N., (1997). Model of global spontaneous activity and local structured activity during delay periods in the cerebral cortex. *Cerebral cortex* 7, 237-252.
- Arieli, A., Shoham, D., Hildesheim, R., & Grinvald, A., (1995). Coherent spatiotemporal patterns of ongoing activity revealed by real-time optical imaging coupled with single-unit recording in the cat visual cortex. *Journal of Neurophysiology* 73, 2072-2093.
- Bazelt, M., M. T. Telenczuk and R. Miles (2016). Single CA3 pyramidal cells trigger sharp waves in vitro by exciting interneurons. *J Physiol* 594, 2565-2577.
- Borges, F. S., Protachevich, P. R., Lameu, E. L., Bonetti, R. C., Iarosz, K. C., Caldas, I. L., Baptista, M. S., & Batista, A. M., (2017). Synchronised firing patterns in a random network of adaptive exponential integrate-and-fire neuron model. *Neural Networks* 90, 1-7.
- Brette, R., Gerstner, W., (2005). Adaptive exponential integrate-and-fire model as an effective description of neuronal activity. *Journal of Neurophysiology* 94, 3637-3642.
- Brunel, N., (2000). Dynamics of sparsely connected networks of excitatory and inhibitory spiking neurons. *Journal of Computational Neuroscience* 8, 183-208.
- Buzsáki, G., & Mizuseki, K., (2014). The log-dynamic brain: how skewed distributions affect network operations. *Nature Reviews Neuroscience* 15, 264-278.
- Compte, A., (2006). Computational and in vitro studies of persistent activity: edging towards cellular and synaptic mechanisms of working memory. *Neuroscience* 139, 135-151.
- Contreras, D., (2004). Electrophysiological classes of neocortical neurons. *Neural Networks* 17, 633-646.
- Cox, D., Lewis, P., (1966). The statistical analysis of series of events.
- Destexhe, A., (2009). Self-sustained asynchronous irregular states and up-down states in thalamic, cortical and thalamocortical networks of nonlinear integrate-and-fire neurons. *Journal of Computational Neuroscience* 27, 493-506.
- Destexhe, A., Rudolph, M., & Paré, D., (2003). The high conductance state of neocortical neurons in vivo. *Nature Reviews Neuroscience* 4, 739.
- Fox, M. D., Snyder, A. Z., Vincent, J. L., Corbetta, M., Van Essen, D. C., & Raichle, M. E., (2005). The human brain is intrinsically organized into dynamic, anticorrelated functional networks. *Proceedings of the National Academy of Sciences of the United States of America* 102, 9673-9678.
- Gabbiani, F., Koch, C., (1998). Principles of spike train analysis. *Methods in Neuronal Modeling* 12, 313-360.
- Gage, F. H., (2004). Structural plasticity of the adult brain. *Dialogues in Clinical Neuroscience* 6, 2.
- Gewaltig, M.-O., (2013). Self-sustained activity, bursts, and variability in recurrent networks. arXiv:1311.1345.
- Giannopoulos, P. and C. Papatheodoropoulos (2013). Effects of mu-opioid receptor modulation on the hippocampal network activity of sharp wave and ripples. *Br J Pharmacol* 168, 1146-1164.
- Greicius, M. D., Krasnow, B., Reiss, A. L., & Menon, V., (2003). Functional connectivity in the resting brain: a network analysis of the default mode hypothesis. *Proceedings of the National Academy of Sciences of the United States of America* 100, 253-258.
- Grün, S., & Rotter, S., (2010). Analysis of parallel spike trains. *Springer*.
- Haider, B., Duque, A., Hasenstaub, A. R., & McCormick, D. A., (2006). Neocortical network activity in vivo is generated through a dynamic balance of excitation and inhibition. *Journal of Neuroscience* 26, 4535-4545.
- Hromádka, T., DeWeese, M. R., & Zador, A. M., (2008). Sparse representation of sounds in the unanesthetized auditory cortex. *PLoS Biology* 6, e16.
- Izhikevich, E. M., (2003). Simple model of spiking neurons. *IEEE Transactions on Neural Networks* 14, 1569-1572.
- Izhikevich, E. M., & Edelman, G. M., (2008). Large-scale model of mammalian thalamocortical systems. *Proceedings of the national academy of sciences* 105, 3593-3598.
- Kaiser, M., & Hilgetag, C. C., (2010). Optimal hierarchical modular topologies for producing limited sustained activation of neural networks. *Frontiers in Neuroinformatics* 4.
- Kriener, B., Enger, H., Tetzlaff, T., Plesser, H. E., Gewaltig, M.-O., & Einevoll, G. T., 2014. Dynamics of self-sustained asynchronous irregular activity in random networks of spiking neurons with strong synapses. *Frontiers in Computational Neuroscience* 8, 187.
- Kumar, A., Schrader, S., Aertsen, A., & Rotter, S., (2008). The high-conductance state of cortical networks. *Neural Computation* 20, 1-43.
- Lindner, B., (2009). A brief introduction to some simple stochastic processes. *Stochastic Methods in Neuroscience*, 1.
- Litwin-Kumar, A., Doiron, B., (2012). Slow dynamics and high variability in balanced cortical networks with clustered connections. *Nature Neuroscience* 15, 1498-1505.
- Maier, N., V. Nimmrich and A. Draguhn (2003). Cellular and network mechanisms underlying spontaneous sharp wave-ripple complexes in mouse hippocampal slices. *J Physiol* 550, 873-887.
- Maimon, G., Assad, J. A., (2009). Beyond Poisson: increased spike-time regularity across primate parietal cortex. *Neuron* 62, 426-440.
- Mantini, D., Perrucci, M. G., Del Gratta, C., Romani, G. L., & Corbetta, M., (2007). Electrophysiological signatures of resting state networks in the human brain. *Proceedings of the National Academy of Sciences* 104, 13170-13175.
- Mastrogiuseppe, F., & Ostojic, S., (2017). Intrinsically-generated fluctuating activity in excitatory-inhibitory networks. *PLoS Computational Biology* 13, e1005498.
- Mizuseki, K. & Buzsaki, G., (2013). Preconfigured, skewed distribution of firing rates in the hippocampus and entorhinal cortex. *Cell Rep.* 4, 1010-1021.
- Mochizuki, Y., Onaga, T., Shimazaki, H., Shimokawa, T., Tsubo, Y., Kimura, R., et al., (2016). Similarity in Neuronal Firing Regimes across Mammalian Species. *Journal of Neuroscience* 36, 5736-5747.
- O'Connor, D. H., Peron, S. P., Huber, D., & Svoboda, K., (2010). Neural activity in barrel cortex underlying vibrissa-based object localization in mice. *Neuron* 67, 1048-1061.
- Ostojic, S., (2014). Two types of asynchronous activity in networks of excitatory and inhibitory spiking neurons. *Nature Neuroscience* 17, 594-600.
- Parga, N., & Abbott, L. F., (2007). Network model of spontaneous activity exhibiting synchronous transitions between up and down states. *Frontiers in Neuroscience* 1, 57-66.
- Pena, R. F. O., Vellmer, S., Bernardi, D., Roque, A. C., & Lindner, B., (2018). Self-consistent scheme for spike-train power spectra in heterogeneous sparse networks. *Frontiers in Computational Neuroscience* 12, 9.
- Peyrache, A., Dehghani, N., Eskandar, E. N., Madsen, J. R., Anderson, W. S., Donoghue, J. A., Hochberg, L. R., Halgren, E., Cash, S. S., & Destexhe, A., (2012). Spatiotemporal dynamics of neocortical excitation and inhibition during human sleep. *Proceedings of the National Academy of Sciences* 109, 17311736.
- Plenz, D., & Aertsen, A., (1996). Neural dynamics in cortex-striatum co-cultures-II. Spatiotemporal characteristics of neuronal activity. *Neuroscience* 70, 893-924.
- Potjans, T. C., & Diesmann, M., (2014). The cell-type specific cortical microcircuit: relating structure and activity in a full-scale spiking network model. *Cerebral Cortex* 24, 785-806.
- Renart, A., Moreno-Bote, R., Wang, X.-J., & Parga, N., (2007). Mean-driven and fluctuation-driven persistent activity in recur-

- rent networks. *Neural Computation* 19, 1-46.
- Rudolph, M., Pospischil, M., Timofeev, I., & Destexhe, A., (2007). Inhibition determines membrane potential dynamics and controls action potential generation in awake and sleeping cat cortex. *Journal of Neuroscience* 27, 5280-5290.
- Sanchez-Vives, M. V., & McCormick, D. A., (2000). Cellular and network mechanisms of rhythmic recurrent activity in neocortex. *Nature neuroscience* 10, 1027-1034.
- Shadlen, M. N., & Newsome, W. T., (1994). Noise, neural codes and cortical organization. *Current Opinion in Neurobiology* 4, 569-579.
- Shu, Y., Hasenstaub, A., & McCormick, D. A., (2003). Turning on and off recurrent balanced cortical activity. *Nature* 423, 288.
- Steriade, M., Nunez, A., & Amzica, F., (1993). A novel slow (< 1 Hz) oscillation of neocortical neurons in vivo: depolarizing and hyperpolarizing components. *Journal of Neuroscience* 8, 3252-3265.
- Steriade, M., Timofeev, I., & Grenier, F., (2001). Natural waking and sleep states: a view from inside neocortical neurons. *Journal of neurophysiology* 85, 1969-1985.
- Stratton, P., & Wiles, J., (2010). Self-sustained non-periodic activity in networks of spiking neurons: The contribution of local and long-range connections and dynamic synapses. *NeuroImage* 52 1070-1079.
- Taub, A. H., Katz, Y., & Lampl, I., (2013). Cortical balance of excitation and inhibition is regulated by the rate of synaptic activity. *Journal of Neuroscience* 33, 14359-14368.
- Timofeev, I., Grenier, F., Bazhenov, M., Sejnowski, T. J., & Steriade, M., (2000). Origin of slow cortical oscillations in deafferented cortical slabs. *Cerebral Cortex* 12, 1185-1199.
- Tomov, P., Pena, R. F., Roque, A. C., & Zaks, M. A., (2016). Mechanisms of self-sustained oscillatory states in hierarchical modular networks with mixtures of electrophysiological cell types. *Frontiers in Computational Neuroscience* 10, 23.
- Tomov, P., Pena, R. F., Zaks, M. A., & Roque, A. C., (2014). Sustained oscillations, irregular firing, and chaotic dynamics in hierarchical modular networks with mixtures of electrophysiological cell types. *Frontiers in Computational Neuroscience* 8, 103.
- van vreeswijk, C. A., & Abbott, L., (1993). Self-sustained firing in populations of integrate-and-fire neurons. *SIAM Journal on Applied Mathematics* 53, 253-264.
- van Vreeswijk, C. A., & Sompolinsky, H., (1998). Chaotic balanced state in a model of cortical circuits. *Neural computation* 10, 1321-1371.
- van Vreeswijk, C. A., & Sompolinsky, H., (1996). Chaos in neuronal networks with balanced excitatory and inhibitory activity. *Science* 274, 1724-1726.
- van vreeswijk, C. A., & Sompolinsky, H., (2004). Irregular activity in large networks of neurons. In Chow, C., Gutkin, B., Hansel, D., Meunier, C., & Dalibard, J. (Eds.) *Methods and Models in Neurophysics*, Amsterdam: Elsevier.
- Vogels, T. P., & Abbott, L. F., (2005a). Signal propagation and logic gating in networks of integrate-and-fire neurons. *The Journal of Neuroscience* 25, 10786-10795.
- Vogels, T. P., & Abbott, L. F., (2005b). Neural network dynamics. *Annual Review of Neuroscience* 28, 357-376.
- Wang, S.-J., Hilgetag, C. C., & Zhou, C., (2011). Sustained activity in hierarchical modular neural networks: self-organized criticality and oscillations. *Frontiers in Computational Neuroscience* 5.
- Wieland, S., Bernardi, D., Schwalger, T., & Lindner, B., (2015). Slow fluctuations in recurrent networks of spiking neurons. *Physical Review E* 92, 040901.